

Band offset determination of the GaAs/GaAsN interface using the DFT method

H-P Komsa¹, E Arola¹, E Larkins², T T Rantala¹

Department of Physics, Tampere University of Technology, Finland
Faculty of Engineering, University of Nottingham, United Kingdom

E-mail: hannu.komsa@tut.fi

Abstract. The GaAs/GaAsN interface band offset is calculated from first principles. The electrostatic potential at the core regions of the atoms is used to estimate the interface potential and align the band structures obtained from respective bulk calculations. First, it is shown that the present method performs well on the well-known conventional/conventional AlAs/GaAs (001) superlattice system. Then the method is applied to a more challenging nonconventional/conventional GaAsN/GaAs (001) system, and consequently type I band lineup and valence-band offset of about 35 meV is obtained for nitrogen concentration of about 3 %, in agreement with the recent experiments. We also investigate the effect of strain on the band lineup. For the GaAsN layer longitudinally strained to the GaAs lattice constant, the type II lineup with a nearly vanishing band offset is found, suggesting that the anisotropic strain along the interface is the principal cause for the often observed type I lineup.

PACS numbers: 71.15.Mb, 73.21.Cd

Submitted to: *J. Phys.: Condens. Matter*

1. Introduction

Since the birth of the band-gap engineering the estimation of the band offsets at interfaces has become of utmost importance. Control of band offsets enables the control of charge carrier flow and confinement, which is a basic requirement in practically all semiconductor device design. Unlike the conventional III-IV semiconductor alloys, whose physical properties change smoothly as a function of the alloying composition, GaAs_{1-x}N_x alloys have attracted a plenty of experimental and theoretical attention due to their unusual physical properties. For example, the incorporation of nitrogen into GaAs drastically reduces the band gap, [1, 2] which makes this material technologically attractive for optoelectronic devices. [3] This feature, together with a peculiar electronic states localization and/or delocalization behaviour near the band edges of GaAsN, [4] have obviously important implications to the band offset properties of the GaAsN/GaAs heterostructure.

Recently, there has been debate on whether GaAsN grown on the GaAs substrate would show a type I [5, 6, 7, 8, 9] or type II [10, 11, 12] band lineup, i.e., whether the GaAsN valence-band maximum (VBM) is above or below the GaAs VBM, respectively, as both results have been obtained experimentally. Apart from the early dielectric model [13], all the computational results support type I lineup [14, 15, 16, 17]. Naturally, whether the band lineup is type I or type II has a dramatic effect on the device performance. Nowadays, it seems to be accepted that the lineup is type I. After all, the devices designed, while expecting a type I lineup, seem to be working. However, the actual amount of the valence-band offset is still unknown, but usually a few tens of meV is assumed. This means that the band gap difference is almost completely on the conduction-band offset.

Band offsets at the interfaces of heterostructures have been calculated with more or less refined methods. Previously, the methods usually concentrated on finding one bulk-specific parameter, which could then be used to determine the lineup. Most important methods are the Anderson affinity rule [18] and Tersoff's theory of effective midgap states [19]. Attempts to determine the VBM in a global energy reference can also be counted to this group. These methods use no information about the interface, and therefore lead to the transitivity law for the valence-band offsets between compound semiconductors as described by Wei and Zunger [20]. This transitivity property holds fairly well for unstrained "natural" band offsets between pure semiconductor compounds [20], but fails in the case of strained layers. A straightforward method would be to calculate complete heterostructure and look at the local densities of states [21], but is practically troublesome. Later on, methods that combine information about the interface from one calculation and information about the two bulk constituent systems from separate calculations, have gained popularity [22, 23, 24, 25]. This method combines the physically valid framework with the computational affordability, which has made it the most used method, and will be our choice, too. These methods can be performed using either semi-empirical or *ab initio* computational framework. Along

with the abundance of computational resources it has become possible to calculate band offsets from first principles at the interface of binary systems [22, 23, 24, 20] and even some tertiary systems [25].

Despite the general interest towards the GaAs/GaAsN material system, the computational considerations are hindered by the low concentration of (randomly substituted) nitrogen in the GaAsN layer, and the polymorphic nature of GaAsN, resulting in the need of a large periodic computational cell. For this reason, previous calculations have been using either $\mathbf{k} \cdot \mathbf{p}$ method [15], tight-binding results fitted to the BAC method [14], or semiempirical pseudopotential methods [16]. Purely *first-principles* calculations have been missing until now. Other notable differences are that in all of these approaches the VBM energies of the bulk material constituents are calculated and these do not consider interface effects, and also the effect of strain due to lattice-matching to the substrate has not been explicitly examined. To solve these problems, we not only need to use large supercells, but also an alternative way to extract the strength of the interface potential.

In this study, we present a revision of the old models modified in a way that the electrostatic potential is determined from the atomic cores. The central part of our model is similar to the one used by Jaffe *et al.* [26] in their α -Cr₂O₃/ α -Fe₂O₃ (0001) interface band offset calculations, containing analogous features from the experimental band-offset measurement technique based on the core-state (x-ray) photoelectron spectroscopy, see, for example, Ref. [27]. This should naturally alleviate the problems mentioned above, and we will show in the following that this is the case. In section 3 we demonstrate the applicability of our method on the well-known AlAs/GaAs system. In addition to the band-offset values, we provide additional insight into the electronic structure of the states near the VBM by looking at the wavefunction localization. Finally, we proceed on to the more challenging case of the GaAsN/GaAs system and carry out a similar analysis there.

2. Models and Methods

In a semiconductor interface, lining up the Fermi-levels causes charge accumulation at the interface, which creates an electric field and subsequently a potential at the interface. Since the energy reference of the band structure can be related to the average electrostatic potential, it is sufficient to estimate the change in the average electrostatic potential through the interface from a heterostructure calculation, and then align the bulk valence-band maxima accordingly to obtain the valence-band offset.

There are several ways to incorporate the concept of the average electrostatic potential into the calculation of the band offset. Bylander and Kleinman [22, 23] used a method where the interfacial double-layer potential (ΔV), induced by the planar average of the difference between the superlattice and the bulk constituent charge densities ($\Delta\rho$), was used along with the bulk constituent Γ_8 eigenvalues of the valence-band maximum, in order to determine the valence-band offset. In the method of Baldeschi *et al.*

[24] running average across the unit cell, along the growth direction, of the xy planar averaged potential is calculated to obtain a slowly varying curve for the potential, from where it is a simple thing to read the potential shifts. In principle, one could also take only one point (any point) from the electrostatic potential and compare that between the interface calculation and the bulk calculation. In practice, due to charge redistribution and geometric relaxations, a well-defined reference point in space should be chosen. An example of such a point would be the potential in the core regions of the ions.

Merely from this reasoning, it is possible to write out the equation for the band offset between the materials X and Y

$$\begin{aligned}\Delta E_v &= (E_v[X] - V_c[X])^b - (E_v[Y] - V_c[Y])^b + (V_c[X] - V_c[Y])^i \\ &= (E_v[X] - E_v[Y])^b + (V_c[X]^i - V_c[X]^b - V_c[Y]^i + V_c[Y]^b) \\ &= \Delta E_v^b + \Delta V_c^i,\end{aligned}\tag{1}$$

where E_v is the valence-band maximum and $V_c[X(Y)]$ is the electrostatic potential at the core of a given type of an atom (anion or cation) located in the material $X(Y)$. Superscripts b and i stand for the bulk and interface calculation, respectively. Finally, ΔE_v^b is the lineup of the VBM between the bulk constituents X and Y , and ΔV_c^i aligns the energy reference by combining the electrostatic potentials at the core of some appropriately chosen anions or cations from the bulk and interface calculations.

Further justification for the use of the electrostatic potential at the atomic core, in aligning the two bulk band structures can be found from the idea of the band offset determination by the core-level photoemission spectroscopy [27]. In this approach, the core levels are measured with respect to the valence-band maxima. At the same time, the change in the core-level energy from one side of the interface (X) to the other (Y) is also measured, so that the valence-band offset ΔE_v at the heterojunction interface is simply given by

$$\Delta E_v = (E_v[X] - E_{cl}[X]) - (E_v[Y] - E_{cl}[Y]) + (E_{cl}[X]^i - E_{cl}[Y]^i),\tag{2}$$

where $E_v[X(Y)]$ and $E_{cl}[X(Y)]$ are the valence-band maximum and core-level energy of the material $X(Y)$, far away from the interface, and $E_{cl}[X(Y)]^i$ is the core-level energy at the $X(Y)$ side of the interface. On the basis of our calculations for the band offset at the interface of the AlAs/GaAs system (see Sec. 3.1 for details), it seems obvious that in the common-anion system the anion core potential can be used to accurately calculate the macroscopic average, as defined by Baldereschi *et al.* [24], of the electrostatic potential across the interface, and therefore to accurately estimate the valence-band offset. Similarly, a cation-related core potential can be used in band-offset calculations for common-cation systems.

Using the core-level energies in determining the band offset is computationally problematic, since this approach requires, if not an all-electron method, at least a method with deep core potentials and subsequently sufficient number of valence electrons active in the calculation. A comprehensive list of band offsets for binary materials calculated with this approach, using the linearized augmented plane wave (LAPW)

method, has been given by Wei and Zunger. [20] For large systems, such methods are computationally prohibitively expensive, and therefore pseudopotential or frozen-core methods (e.g. the projector-augmented wave method, PAW) would be more suitable ones. The electrostatic potential at each ion (“the core potential”) is calculated by placing a test charge at each ion and calculating in the usual way

$$V_c(\mathbf{R}_n) = \int V(\mathbf{r})\rho_{test}(|\mathbf{r} - \mathbf{R}_n|)d^3\mathbf{r}, \quad (3)$$

i.e., we estimate the test-charge distribution weighted average of the electrostatic potential, a typical core electron would experience. More precisely, the integral is calculated over a spatially extended spherically symmetric region whose radius is related to the PAW core radius. The norm of the test charge distribution is constrained to one. The radii for the test charge distributions are taken 1.03 Å for gallium, 1.06 Å for arsenic and 0.75 Å for nitrogen.

Although this method can be applied to any material system, with or without a lattice-matched interface, it is especially useful in calculating the band offset of the nitrogen dilute and low-concentration GaAsN alloy with respect to GaAs, as can be seen from the following points. First of all, a laterally wide computational cell is required for these nitride material systems, but, on the other hand, it is known that the macroscopic average of the electric dipole-related electrostatic potential becomes saturated rapidly away from the interface, and therefore only a few layers of the material is needed in the longitudinal direction to estimate the interface potential. Second, the calculation of the running average of the planar-averaged electrostatic potential over conventional 8-atom unit cells is ill-defined since in the dilute and low-concentration nitride systems the atomic positions around the nitrogen atoms are strongly displaced from their ideal positions in the zinc-blende lattice structure. Third, the valence-band offset in the GaAsN/GaAs systems is known to be very small, so reading the band offset from the layer-projected local density of states (LDOS) is practically impossible, particularly due to the relatively small thickness of these layers. Finally, the method used for the band offset calculation for the AlAs/GaAs system in Refs. [22] and [23], requires that the planar averages of both the bulk and superlattice electrostatic potentials have been computed using the same \mathbf{k} -point mesh, and that identical lattice geometries have been used in the both cases.

In our studies presented here, all calculations were performed within the density functional theory (DFT) framework using a plane-wave basis as implemented in the code VASP (Vienna *ab initio* simulation package) [28, 29, 30]. The atomic core regions are described using projector-augmented waves (PAW) with the 3*d* electrons of gallium explicitly included in the calculation. The local density approximation (LDA) of Ceperley and Alder is used, as parametrized by Perdew and Zunger [31, 32].

The spin-orbit coupling (SOC), making the computation a lot more time consuming, is not included in our band-offset calculations. However, the following points obviously justify us omitting the SOC from our calculations. Firstly, on the basis of our band-offset test calculations for the AlAs/GaAs system, using a supercell composed of 4 + 4

unit cells, it seems that there is hardly any change in the Coulomb potential behaviour across the interface when the SOC is included (e.g. the planar averaged quantity ΔV_C^i of Eq. (1) changes only about 1 meV when the SOC is switched on). Secondly, our test calculations on the AlAs/GaAs system show that the valence-band offset increases by some 13 meV when the SOC is included. It is noticeable that this change in the band offset is only about one third of the difference between the spin-orbit (SO) -splitting at the VBM (Δ_0) in GaAs (0.34 eV) and in AlAs (0.30 eV). Finally, the electroreflectance experiments by Perkins *et al.* [33] for GaAs_{1-x}N_x alloys reveal that the SO-splitting at the VBM stays nearly constant for $0 < x < 3\%$, being 0.33 eV for $x = 2.2\%$. Also, our calculations with the SOC give very similar Δ_0 values of 0.33 eV and 0.31 eV for the isotropic bulk GaAs_{1-x}N_x ($x = 3.125\%$) and for GaAs_{1-x}N_x ($x = 3.125\%$) laterally matched with GaAs, respectively. Given that the abovementioned *ad hoc* “one third”-rule can be transferred also to the GaAsN/GaAs system, we can conclude that the omission of the SOC from our calculations causes less than $(0.34 \text{ eV} - 0.31 \text{ eV})/3 = 10 \text{ meV}$ error to the band-offset result for the GaAsN/GaAs interface [34].

Since the DFT works reliably for the ground state and the LDA is known to seriously underestimate the fundamental band gap, values of the conduction-band offset from these calculations can not be expected to be reliable. However, the knowledge of the valence-band offset makes it possible to estimate the conduction-band offset if the band gaps are experimentally known.

3. Results

We begin by testing our method on the well-known AlAs/GaAs material system. We compare the results from two different methods. In the first method, the interface potential has been estimated using the electrostatic potential at the atomic cores [see Eq. (3)], and in the second one using the average electrostatic potential technique of Ref. [24]. Naturally, comparison to previous results in the literature is also given.

3.1. AlAs/GaAs interface

A good review of the experimental data of the band offset for the AlAs/GaAs system is given by Vurgaftman *et al.* [35]. A split of 65:35 between conduction- and valence-band discontinuities is generally agreed upon. The direct band gap for GaAs is 1.424 eV and for AlAs about 2.95 eV, resulting in a valence-band offset of about 0.53 eV at 300 K. These results show no significant differences between the 0 K and 300 K temperatures. The LAPW result obtained by Wei is 0.51 eV [20].

Our computational cell is 16 cubic unit cells long and one unit cell wide in the two lateral directions, resulting in a total of 128 atoms. The first 8 unit cells form the AlAs layer and the following 8 unit cells form the GaAs layer. The lattice constant is chosen so that the system is lattice matched to GaAs in all directions. Even though the supercell size has not been optimized, the atomic geometry within the cell has been relaxed. As

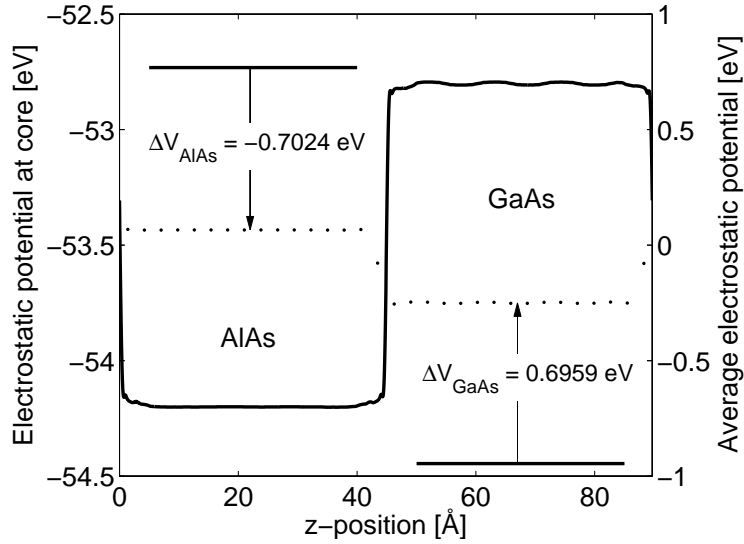


Figure 1. Electrostatic potential at the cores of arsenic atoms in the supercell of the AlAs/GaAs system (dotted line), and the corresponding values in the AlAs and GaAs bulk constituents (solid horizontal lines) [energy scale on the left]. Also shown is the macroscopically averaged electrostatic potential (solid line, see Ref. [24]) where the averaging steps along the longitudinal direction of the supercell have been carried out over the 8-atom unit cells [energy scale on the right].

the computationally relaxed GaAs lattice constant is 5.605 \AA , this corresponds to layers of about 4.5 nm thickness in the $\langle 100 \rangle$ direction. This is in the limit of experimentally achievable quantum well widths. $4 \times 4 \times 2$ Monkhorst-Pack \mathbf{k} -point set is used to calculate the total energy and atomic geometry relaxation, and a $9 \times 9 \times 3$ \mathbf{k} -point set is used to calculate the density of states.

First, we consider our method of lining up the electrostatic potentials at the cores of arsenic atoms. In figure 1 the potential at the arsenic core is plotted along the longitudinal direction of the supercell together with the corresponding bulk values. As compared to the bulk, in the heterostructure calculation, the arsenic core potential on the GaAs side is increased by 0.6959 eV and on the AlAs side it is decreased by -0.7024 eV , resulting in $\Delta V_c^i = 1.3983 \text{ eV}$. The valence-band maximum is at $E_v[\text{GaAs}] = 3.1608 \text{ eV}$ in the GaAs bulk and $E_v[\text{AlAs}] = 4.0412 \text{ eV}$ in the AlAs bulk, Eq. 1 giving out the band offset $\Delta E_v = 0.5179 \text{ eV}$.

Next, we calculate the macroscopically averaged electrostatic potential along the longitudinal direction of the supercell following the method of Baldereschi [24]. The result for this is also shown in figure 1. The average over the averaged macroscopical potential is $\langle \bar{V}[\text{GaAs}] \rangle = 0.7000 \text{ eV}$ on the GaAs side of the supercell and $\langle \bar{V}[\text{AlAs}] \rangle = -0.7003 \text{ eV}$ on the AlAs side, yielding almost the same interface potential of $\Delta V^i = 1.4002 \text{ eV}$. The average of the electrostatic potential of the bulk is zero [in this case ΔV^i corresponds to ΔV_c^i of Eq. (1)], so we can readily shift the bulk VBM values with this, yielding $\Delta E_v = 0.5198 \text{ eV}$. These results are very close to the experimental values and

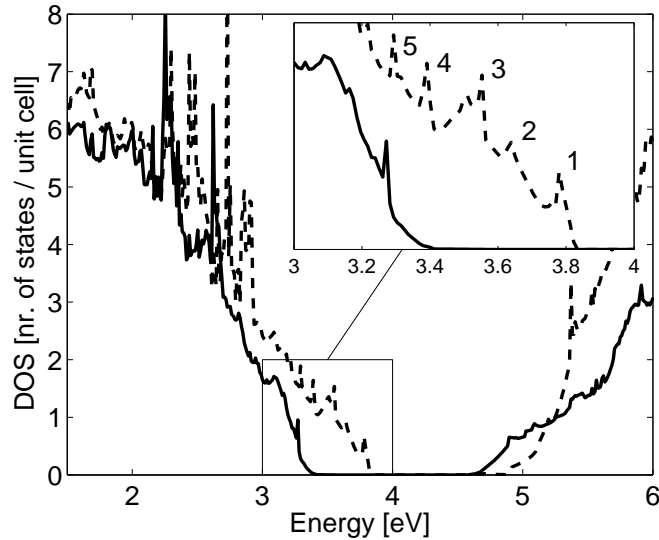


Figure 2. The local DOS of one 8-atom unit-cell wide slice from the AlAs layer (solid line) and GaAs layer (dashed line) of the AlAs/GaAs (001) $1 \times 1 \times 16$ supercell.

that from the LAPW method. It is clear that the two methods produce very similar results and that our “core level” method appears to be well justified.

At this point, we briefly mention that the difference between our computational lattice constants of AlAs ($a = 5.635 \text{ \AA}$) and GaAs ($a = 5.605 \text{ \AA}$) is 0.03 \AA , while the corresponding experimental difference is only 0.008 \AA . This results in a slightly overestimated strain of the AlAs/GaAs system in our calculations.

It has been shown in the previous studies that only a few atomic layers of material is sufficient for the potential to become saturated away from the interface (cf. e.g. Ref. [24]). This is also evident from figure 1. This turns out to be a case, also in the GaAsN/GaAs system (see section 3.2).

In order to justify the analysis of the wavefunctions on the GaAs/GaAsN system in the next section, we take a closer look at the one-electron states in the AlAs/GaAs (001) superlattice system. Firstly, in figure 2, we show the local DOS projected onto one 8-atom unit-cell wide slice taken in the middle of the AlAs and GaAs layers. In principle, one could also estimate the band offset from this figure (around 0.5 eV). However, it is difficult to extract precise values, and to be exact, this is not the band offset, but the difference between the highest quantum well (QW) confined state and the highest unconfined state. This value is smaller than the band offset but it should approach the band offset as the width of the QW increases. However, this is an impractical method, because of the prohibitively large computational volume required. Furthermore, in figure 3, we show the envelope-like functions [36] of the highest confined hole states at the Γ point. To be more precise, the localization of the superlattice wavefunction (Bloch wave), projected onto the slice of half the 8-atom unit cell, is plotted along the longitudinal direction of the supercell and vertically shifted to the corresponding

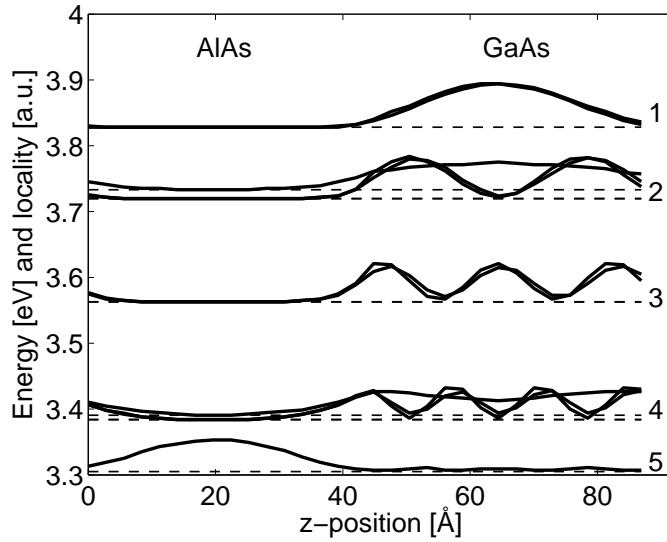


Figure 3. Envelope-like functions of the highest valence-band states at the Γ point, showing the localization of these states. Dashed lines show the energy levels. Envelope-like functions are in arbitrary units, whose zero level has been defined by their corresponding energy levels.

energy eigenvalue. It is clear, that this slice-projected localization of the wavefunction in one region of a heterostructure means confinement of the charge carriers at that region, and here particularly confinement of holes due to the QW structure. The five LDOS peaks in the inset of figure 2, are derived from the centre-slice of the GaAs slab, and can obviously be related to the confined mini-band states of the AlAs/GaAs (001) superlattice structure.

3.2. GaAsN/GaAs interface

The practical nitrogen concentration in GaAsN is usually only a few percent due to the miscibility gap restricting the growth. If one arsenic is replaced by a nitrogen in a 64-atom cubic supercell it corresponds to a nitrogen concentration of about 3 %. Therefore, our bulk calculations have been performed with a 64-atom supercell and using $2 \times 2 \times 2$ \mathbf{k} -space sampling. Since there is only one nitrogen in the 64-atom supercell, for the minimal construction of the heterostructure supercell we need two 64-atom GaAsN supercells and preferably same amount of GaAs, giving out a 256-atom supercell. Because the GaAsN layers have to be lattice matched to GaAs in the lateral directions, this also requires that the longitudinal lattice constant has to be optimized to give the minimum total energy. Since the 256-atom supercell calculations are computationally expensive we carry out the longitudinal lattice constant optimization of the bulk and interface regions separately. Interface effects on the cell size are estimated from a 128-atom supercell and $2 \times 2 \times 1$ \mathbf{k} points. When building a 256-atom heterostructure supercell, we interlace the GaAsN and GaAs bulk geometries from their 64-atom bulk calculations and GaAsN/GaAs (001)

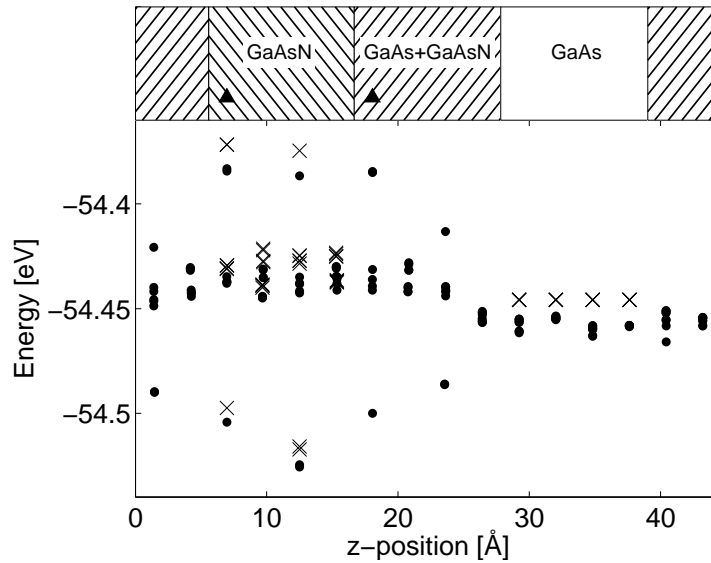


Figure 4. Electrostatic potential at cores of arsenic atoms along the longitudinal direction of the GaAsN/GaAs (001) supercell. The dots are from the superlattice calculation and the crosses are from the GaAsN and GaAs bulk constituent calculations. On the top of the picture is depicted a construction of the $2 \times 2 \times 8$ supercell. Triangles show the positions of the two nitrogen atoms in the supercell.

interface geometries from the 128-atom calculation. Construction of this supercell can be seen on the top of figure 4. After this we perform one more relaxation for the ions inside the 256-atom supercell without optimization of the longitudinal lattice constant.

Although it is difficult to say what the "effective nitrogen concentration" of the GaAsN layer in this supercell is, we assume that the roughly 3 % nitrogen concentration of our GaAsN bulk calculation would be a good estimate. It is worth pointing out that the real GaAsN alloy has a substitutionally random nitrogen distribution, while the GaAsN phase in our GaAsN/GaAs (001) superlattice calculation repeats itself periodically, and therefore defines an ordered distribution of N atoms.

The electrostatic potential at the cores of arsenic atoms is shown in figure 4 for both interface and bulk calculations. One can see saturation, when moving away from the interface, in the potential values, in both the GaAsN and GaAs layers. The single isolated potential values below the mean are due to the arsenic atoms between nitrogen atoms along the (110) directions. Those above the mean are due to the arsenic atoms between nitrogen atoms along the (100) directions.

While averaging over the arsenic core potentials in the middle of the GaAs and GaAsN regions, a suitable volume has to be selected. We have tested three different volumes on the GaAsN side of the supercell: "mid1" has only one monolayer of arsenic atoms between the nitrogen atoms, "mid3" has 3 monolayers of arsenic atoms between the nitrogen atoms, and "64c" has 4 monolayers of arsenic atoms consisting of the same arsenic atoms as in the original 64-atom GaAsN supercell that was embedded into the heterostructure supercell. In the same way, the averaging volumes "mid1", "mid3", and

Table 1. Band offsets calculated with different averaging models.

Longitudinally relaxed superlattice						
model	VBM		$V_c^i[X(Y)] - V_c^b[X(Y)]$		ΔV_c^i	ΔE_v
	GaAsN	GaAs	$X \equiv \text{GaAsN}$	$Y \equiv \text{GaAs}$		
mid1	3.1920	3.1608	-0.0115	-0.0143	0.0028	0.0340
mid3	3.1920	3.1608	-0.0074	-0.0117	0.0043	0.0355
64c	3.1920	3.1608	-0.0076	-0.0118	0.0042	0.0354
Longitudinally lattice-matched superlattice						
model	VBM		$V_c^i[X(Y)] - V_c^b[X(Y)]$		ΔV_c^i	ΔE_v
	GaAsN	GaAs	$X \equiv \text{GaAsN}$	$Y \equiv \text{GaAs}$		
mid1	3.0499	3.1608	0.0507	-0.0576	0.1083	-0.0026
mid3	3.0499	3.1608	0.0500	-0.0572	0.1072	-0.0037
64c	3.0499	3.1608	0.0489	-0.0567	0.1056	-0.0053

”64c”, will be defined on the GaAs side of the supercell.

Valence-band maxima, changes in the averaged electrostatic potential, and finally the band offsets are collected in table 1. We can see, that using different averaging models, has only a minor effect on the band offset. A type I band offset of about 35 meV is obtained in the longitudinally relaxed case. Looking at the results of table 1, for the longitudinally relaxed superlattice case, one could even go as far as to claim that the 3 % nitrogen concentration is dilute enough such that ΔV_c^i could be approximated to be zero. This assumption can obviously be transferred to calculate the band offset only from the bulk VBM values in the case of the GaAsN/GaAs superlattice containing an even more nitrogen-dilute GaAsN layer. We have carried out a one- \mathbf{k} -point (Γ) calculation for a 216-atom cubic supercell (composed of $3 \times 3 \times 3$ conventional 8-atom GaAs unit cells and one nitrogen atom) lattice-matched to the GaAs bulk in two lateral directions (along the interface) and relaxed in the third one (perpendicular to the interface). In this case, the isotropic nitrogen concentration, being 0.93 % in the GaAsN layer, leads to the VBM value of 3.1673 eV and the valence-band offset of about 7 meV.

Although the GaAs bulk VBM is located at $E_v[\text{GaAs}] = 3.1608$ eV at the Γ point, and is triply degenerate (when the SOC not included), the corresponding eigenvalues for the GaAsN bulk with SOC have about 48 meV split due to the anisotropic strain. Therefore, even if the upper GaAsN valence band is located higher than the GaAs VBM, and the type I band offset is observed, the lower GaAsN valence band is located at slightly lower energy than the GaAs VBM, suggesting only a weak charge carrier confinement in the GaAsN layer of the GaAsN/GaAs (001) superlattice.

We also tested what would happen if the anisotropic strain is removed. For this purpose we longitudinally stretched the heterostructure supercell to match the GaAs lattice constant, although unfortunately this still leaves the isotropic strain component left. The data of the longitudinally lattice-matched case is also shown in table 1 and a

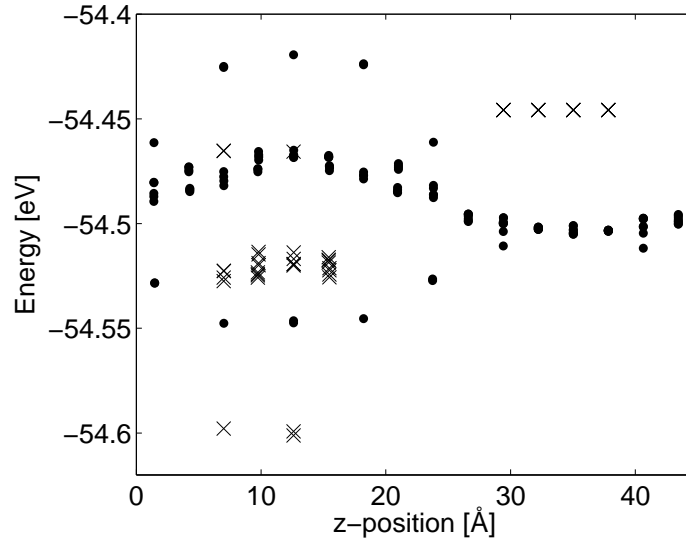


Figure 5. Electrostatic potential at the cores of arsenic atoms along the longitudinal direction of the GaAsN/GaAs (001) longitudinally lattice-matched supercell. The dots are from the interface calculation and the crosses are from the GaAsN and GaAs bulk constituent calculations.

picture of the electrostatic potential distribution at the cores of arsenic atoms is shown in figure 5. In this case the band offset is changed to type II, but with a nearly vanishing band offset of about 4 meV.

Our results are in agreement with the experimental results of Egorov [9] and also with the computational results of Lindsay [14] and Bellaiche [16]. Egorov gives the band offset of 15 ± 5 meV for the nitrogen concentration of about 2 %. By applying linear interpolation onto this experimental value we get about 25 meV for the 3 % concentration and about 7 meV for the 1 % concentration. From the data of Bellaiche the band offset of about 20 – 30 meV for the case of 3 % concentration, can be estimated in good agreement with our results. Finally, Lindsay gives a formula for the VBM evolution as $E_v(x) = 0.2x$ eV, and therefore for the case of the 3 % concentration, this means about 6 meV value for the band offset, providing that the contribution of the interfacial Coulomb potential change ΔV_c^i could be ignored. Additionally, Egorov also presents a band-offset estimate for an unstrained case, which is 0 ± 5 meV (for the 2 % nitrogen concentration). The tendency seen in our computational observations matches with this experimental behaviour, and also with the recent tight-binding (TB) empirical band offset calculations by Shtinkov *et al.* [37] for the GaAs_{1-x}N_x/GaAs (001) QW system, in the case where the anisotropic strain was removed.

If the isotropically strained GaAsN layer in the GaAsN/GaAs superlattice leads to a band offset very close to zero, then our results give a strong indication that the type I lineup of this material system is mainly caused by the VBM split states due to the anisotropic strain of the GaAsN layer, and without this strain there occurs no band

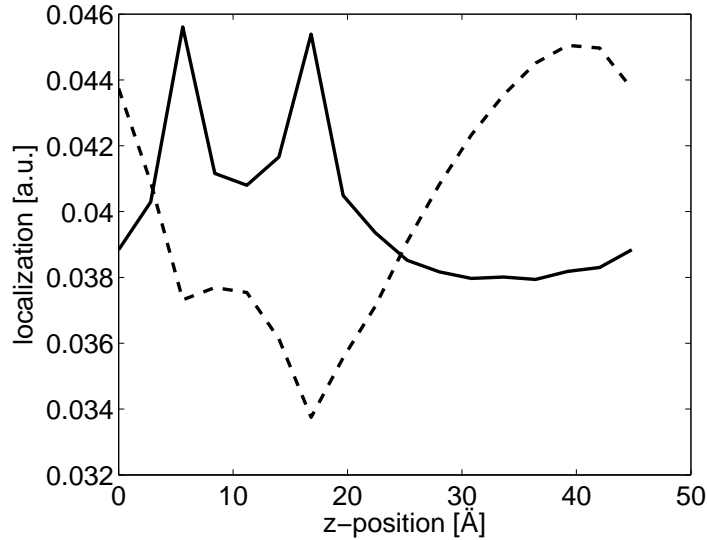


Figure 6. Localization of the upmost valence-band states along the longitudinal direction of the the supercell, presented in the same way as in figure 3. The solid line is from the longitudinally relaxed superlattice and the dashed line is from the longitudinally lattice-matched superlattice.

offset, or even a type II lineup can be expected in this situation.

More insight can be gained by looking at the wavefunction localization along the longitudinal direction of the supercell for the uppermost valence-band state (located at the Γ point) in both the longitudinally relaxed and the longitudinally lattice-matched cases. This is shown in figure 6. In the case of the longitudinally relaxed supercell, this state is localized strongly on the nitrogen atoms, and on the average residing on the GaAsN side, as is natural if the GaAsN layer in the GaAsN/GaAs (001) superlattice is supposed to feature type I lineup. In the case of the longitudinally lattice-matched supercell, the situation is the opposite. The wavefunction is now localized on the GaAs side as is natural for the type II lineup. Interestingly, in this case charge is depleted from the nitrogen-localized states region in the GaAsN layer of the supercell, into the GaAs layer. This is directly reflected in the change of the interfacial Coulombic potential term ΔV_c^i of Eq. (1), which furthermore derives from the change in the induced electric dipole across the interface. Remarkably, it can be seen from table 1 that this change in ΔV_c^i is rather large, being more than 100 meV, when going from the longitudinally relaxed superlattice to longitudinally lattice-matched one. Obviously, the electron charge localization behaviour at the nitrogen atoms, much responsible for the change in ΔV_c^i , is a result of a subtle interplay between the QW-like confinement, strain, and polymorphic nature of the GaAsN alloy.

In view of our computational approach, we briefly comment in the following our band-offset calculations between the AlAs/GaAs (001) and GaAsN/GaAs (001) superlattice cases.

Figure 1, referring to the case of the AlAs/GaAs (001) superlattice, clearly indicates that the macroscopically averaged potential, as well as the core potential at the As sites, change rapidly along the z direction near the interface, and then quickly saturate to an essentially constant value. It is exactly this kind of behaviour in the electrostatic potentials that can be used to define an "abrupt interface" between two semiconductors, and typically exists between two "conventional" isoelectronic semiconductors (e.g. the GaAs $_{1-x}$ P $_x$ alloy).

However, as Figures 4 and 5 show, the situation in the case of the GaAsN/GaAs (001) superlattice, is quite the opposite. Due to the slow spread-out of the core potential at As sites (in the z direction) across the middle of the supercell, the "thickness" and location of the interface, from the electronic structure viewpoint, are not so well-defined anymore. Furthermore, obviously owing to the polymorphic nature of GaAsN alloy and sensitive localization properties of the VBM states at the nitrogen atoms in the GaAsN/GaAs superlattice, there are rather large fluctuations at the core potential of the As sites. However, the planar averaged quantity of the As core potentials obviously leads to a smooth behaving curve along the z direction, with two well-defined plateaus (one in the GaAsN layer, and the other one in the GaAs layer) which can be used to determine ΔV_c^i .

From these computational observations we can conclude that the concept of the band offset may become ill-defined for the GaAsN/GaAs superlattice, particularly in the case where the GaAsN layer is very thin.

Finally, we briefly discuss the relationship between the atomic- and electronic structural properties and optical properties in GaAsN/GaAs systems. First of all, the optical studies by Pan *et al.* [38] on GaAs $_{1-x}$ N $_x$ layers on the GaAs (001) substrate and by Gao *et al.* [39] on the GaAsN/GaAs QW structure in connection with the strain-compensating InAs layers clearly demonstrated that optical properties, in terms of photoluminescence (PL) emission, are highly sensitive to the strain state and its relaxation of the GaAsN layer. Secondly, Luo *et al.* [40] observed a strong excitation energy- and rapid thermal annealing (RTA) sensitive feature at the photon energy of 1.385 eV (denoted as M in their paper) in the PL spectra of the GaAsN/GaAs quantum well samples, which they interpreted to be due to the interface-related localized exciton emission. Interestingly, this PL feature can be greatly reduced by the RTA treatment, therefore improving the "optical quality" of the GaAsN/GaAs interface via reducing the localization traps at the interfaces. Therefore, on the basis of our band offset calculations and these experimental observations, we can conclude that the strain state of the GaAsN layer in the GaAsN/GaAs QW largely influences both its band offset (type of the band offset and its value) as well as PL properties. Furthermore, it is obvious that the localized excitonic trap states at the GaAsN/GaAs interface have effect on, not only on the PL spectra, but also on the band offset itself.

4. Conclusions

We have presented an alternative way of extracting the interface potential at a heterostructure interface from the electrostatic potentials estimated at the atomic cores. This method is suitable for the systems with large geometric displacements and not so well-defined interface, in terms of its location and distribution along the growth direction, i.e. the interface abruptness. After performing tests with the well-known AlAs/GaAs system we have applied it to study the technologically interesting GaAsN/GaAs interface.

We find a type I lineup with a band offset of about 35 meV for GaAsN layer of about 3 % nitrogen concentration laterally lattice matched to GaAs and about 7 meV for the 1 % layer. Moreover, a type II lineup with the band offset close to zero is found for a GaAsN layer strained to fit the GaAs lattice constant in all directions. Therefore, it is to be expected that the type I band offset is largely due to the VBM split caused by the anisotropic strain. We also studied the nitrogen localization by looking at the envelope-like wavefunctions of the VBM states.

We have recently started atomic and electronic structural studies on the quinary GaInAsNX/GaAs material system (X is some appropriate impurity additive), which for X=Sb, has recently been demonstrated to be among the best candidates for semiconductor lasers operating at wavelengths longer than 1.3 μm [41, 42].

Acknowledgments

We are thankful for the Centre for Scientific Computing (CSC) in Finland and Material Sciences National Grid Infrastructure (M-grid, akaatti) for the computational resources.

References

- [1] M. Weyers, M. Sato, and H. Ando. *Jpn. J. Appl. Phys., Part 2*, 31:853, 1992.
- [2] S.-H. Wei and A. Zunger. *Phys. Rev. Lett.*, 76:664, 1996.
- [3] *Semicond. Sci. Technol.*, 17:741, 2002. A special review issue.
- [4] P. R. C. Kent and A. Zunger. *Phys. Rev. Lett.*, 86:2613, 2001.
- [5] P. Krispin, S. G. Spruytte, J. S. Harris, and K. H. Ploog. *J. Appl. Phys.*, 88:4153, 2000.
- [6] Y. Zhang, A. Mascarenhas, H. P. Xin, and C. W. Tu. *Phys. Rev. B*, 61:7479, 2000.
- [7] P. J. Klar, H. Grüning, W. Heimbrodt, J. Koch, W. Stolz, P. M. A. Vicente, A. M. Kamal Saadi, A. Lindsay, and E. P. O'Reilly. *Phys. Stat. Sol. B*, 223:163, 2001.
- [8] I. A. Buyanova, W. M. Chen, and B. Monemar. *MRS Internet J. Nitride Semicond. Res.*, 6:2, 2001.
- [9] A. Yu. Egorov, V. A. Odnoblyudov, N. V. Krizhanovskaya, V. V. Mamutin, and V. M. Ustinov. *Semiconductors*, 36:1355, 2002.
- [10] T. Kitatani, M. Kondow, T. Kikawa, Y. Yazawa, M. Okai, and K. Uomi. *Jpn. J. Appl. Phys.*, 38:5003, 1999.
- [11] B. Q. Sun, D. S. Jiang, X. D. Luo, Z. Y. Xu Z. Pan, L. H. Li, and R. H. Wu. *Appl. Phys. Lett.*, 76:2862, 2000.
- [12] J. F. Chen, C. T. Ke, P. C. Hsieh, C. H. Chiang, W. I. Lee, and S. C. Lee. *J. Appl. Phys.*, 101:123515, 2007.

- [13] S. Sakai, Y. Ueta, and Y. Terauchi. *Jpn. J. Appl. Phys.*, 32:4413, 1993.
- [14] A. Lindsay and E. P. O'Reilly. *Solid State Communications*, 112:443, 1999.
- [15] J. Wu, W. Walukiewicz, K. M. Yu, J. D. Denlinger, W. Shan, J. W. Ager III, A. Kimura, H. F. Tang, and T. F. Kuech. *Phys. Rev. B*, 70:115214, 2004.
- [16] L. Bellaiche, S.-H. Wei, and A. Zunger. *Phys. Rev. B*, 54:17568, 1996.
- [17] A. Gueddim and N. Bouarissa. *Appl. Surf. Sci.*, 253:7336, 2007.
- [18] R. L. Anderson. *IBM J. Res. Dev.*, 4:283, 1960.
- [19] J. Tersoff. *Phys. Rev. B*, 30:4874, 1984.
- [20] S.-H. Wei and A. Zunger. *Appl. Phys. Lett.*, 72:2011, 1998.
- [21] J. M. Bass, M. Oloumi, and C. C. Matthai. *J. Phys.: Condens. Matter*, 1:10625, 1989.
- [22] D. M. Bylander and L. Kleinman. *Phys. Rev. B*, 36:3229, 1987.
- [23] D. M. Bylander and L. Kleinman. *Phys. Rev. Lett.*, 59:2091, 1987.
- [24] A. Baldereschi, S. Baroni, and R. Resta. *Phys. Rev. Lett.*, 61:734, 1988.
- [25] X. H. Zhang, S. J. Chua, S. J. Xu, and W. J. Fan. *J. Phys.: Condens. Matter*, 10:577, 1998.
- [26] J. E. Jaffe, M. Dupuis, and M. Gutowski. *Phys. Rev. B*, 69:205106, 2004.
- [27] E. A. Kraut, R. W. Grant, J. R. Waldrop, and S. P. Kowalczyk. *Phys. Rev. Lett.*, 44:1620, 1980.
- [28] G. Kresse and J. Hafner. *Phys. Rev. B*, 47:558, 1993.
- [29] G. Kresse and J. Furthmüller. *Comput. Mat. Sci.*, 6:15, 1996.
- [30] G. Kresse and J. Furthmüller. *Phys. Rev. B*, 54:11169, 1996.
- [31] D. M. Ceperley and B. J. Alder. *Phys. Rev. Lett.*, 45:566, 1980.
- [32] J. P. Perdew and A. Zunger. *Phys. Rev. B*, 23:5048, 1981.
- [33] J. D. Perkins, A. Mascarenhas, Y. Zhang, D. J. Friedman, J. M. Olson, and S. R. Kurtz. *Phys. Rev. Lett.*, 82:3312, 1999.
- [34] When estimating the correction of including the spin-orbit coupling (SOC), into the band offset at the interface, we have to notice that not only the SOC-split valence levels of the two separate semiconductor materials determine the band offset at their heterojunction, but also the strain at the interface will couple in a complicated manner to these individual SOC-split valence states.
- [35] I. Vurgaftman, J. R. Meyer, and L. R. Ram-Mohan. *J. Appl. Phys.*, 89:5815, 2001.
- [36] The concept of the “envelope-like function” we use here, is not directly related to its standard definition of “envelope function” which appears in the envelope function approximation in the framework of the effective mass approximation for electrons and holes in the QW (for further details, see, for example, Chapter 9 of reference [43]).
- [37] N. Shtinkov, S. Turcotte, J. N. Beaudry, P. Desjardins, and R. A. Masut. *J. Vac. Sci. Technol. A*, 22:1606, 2004.
- [38] Z. Pan, Y. T. Wang, L. H. Li, H. Wang, Z. Wei, Z. Q. Zhou, and Y. W. Lin. *J. Appl. Phys.*, 86:5302, 1999.
- [39] Q. Gao, H. H. Tan, C. Jagadish, B. Q. Sun, M. Gal, L. Ouyang, and J. Zou. *Appl. Phys. Lett.*, 84:2536, 2004.
- [40] X. D. Luo, P. H. Tan, Z. Y. Xu, and W. K. Ge. *J. Appl. Phys.*, 94:4863, 2003.
- [41] F. Ishikawa, E. Luna, A. Trampert, and K. H. Ploog. *Appl. Phys. Lett.*, 89:181910, 2006.
- [42] Jr. J. S. Harris. *J. Cryst. Growth*, 278:3, 2005.
- [43] P. Y. Yu and M. Cardona. *Fundamentals of Semiconductors*. Springer, third edition, 2001.